Inorg. Chem. **2007**, *46*, 1847−1855

Continuous-Wave and Pulse EPR Study of the Copper(II) Complex of N-Confused Tetraphenylporphyrin: Direct Observation of a σ Metal−Carbon Bond

Carlos Calle, Arthur Schweiger,[†] and George Mitrikas*

Laboratory of Physical Chemistry, Department of Chemistry and Applied Biosciences, ETH-Zurich, CH-8093 Zurich, Switzerland

Received November 16, 2006

N-confused or inverted porphyrins, a family of porphyrin isomers that contain a confused pyrrole ring connected through its α and β' positions in the macrocycle, exhibit unique physical and chemical properties, like, for instance, the ability to stabilize unusual oxidation states of metals due to the reactivity of the inverted pyrrole. In this Article, a combined multifrequency continuous-wave and pulse electron paramagnetic resonance (EPR) study of the copper(II) complex of N-confused tetraphenylporphyrin (TPP) is presented. By use of pulse EPR methods like ENDOR and HYSCORE, the magnetic interactions between the unpaired electron of the compound and the surrounding nitrogen nuclei were revealed. Through ^{13}C labeling of the macrocycle, a detailed study of the carbon hyperfine interaction became possible and provided further insight into the character of the metal–carbon bond. The observed hyperfine couplings of the ligand atoms in the first coordination sphere showed the presence of a remarkably strong σ Cu–C bond and allowed for a detailed analysis of the spin delocalization over the porphyrin macrocycle. Interestingly, it was found that the observed delocalization is approximately 11% larger than the corresponding one for CuTPP.

Introduction

N-confused porphyrin (NCP, also known as inverted or carbaporphyrin) is a relatively new isomer of the porphyrin family that contains a C−H unit in the coordination core.[1−4] This macrocycle with a CNNN set of donors exhibits unique chemical properties because it can stabilize unusual oxidation states of metal ions.[5] In addition, the outer nitrogen or carbon atoms of the inverted pyrrole can participate in an outer metal coordination[6] or a direct connection of aromatic subunits,[7] resulting in supramolecular assemblies with very interesting potential applications. More interestingly, NCPs have received increased attention because of their remarkable tendency to form unique organometallic compounds. So far, several stable transition-metal complexes of NCP have been synthesized,[2] including copper(II) N-confused tetraphenylporphyrin [Cu^{II}(NCTPP); Chart 1].[8]

Our initial motivation for studying this paramagnetic compound was triggered by the presence of the rare metal−carbon bond. The characterization of the bonding situation can be very useful for understanding the reactivity of organometallic compounds. Continuous-wave (CW) and pulse electron paramagnetic resonance (EPR) spectroscopy can give unique information about the covalent character of the metal−ligand bonds by measuring the magnetic interactions between the unpaired electron of the complex and the magnetic nuclei of the macrocycle. Up to now, only a few paramagnetic NCP complexes have been studied by EPR methods.[8,9] Recently, by using conventional CW and advanced pulse EPR methods like hyperfine sublevel correla-

* To whom correspondence should be addressed. E-mail: mitrikas@phys.chem.ethz.ch. Tel.: (+41) 44-632-4443. Fax: (+41) 44-632-1021.
[†] Deceased on January 4, 2006.

(1) Chmielewski, P. J.; Latos-Grażyński, L. *Coord. Chem. Rev.* **2005**, *249*, 2510−2533.
(2) Harvey, J. D.; Ziegler, C. J. *Coord. Chem. Rev.* **2003**, *247*, 1−19.
(3) Furuta, H.; Maeda, H.; Osuka, A. *Chem. Commun.* **2002**, 1795−1804.
(4) Pushpan, S. K.; Venkatraman, S.; Anand, V. G.; Sankar, J.; Rath, H.; Chandrashekar, T. K. *Proc. Indian Acad. Sci. Chem. Sci.* **2002**, *114*, 311−338.
(5) Maeda, H.; Ishikawa, Y.; Matsuda, T.; Osuka, A.; Furuta, H. *J. Am. Chem. Soc.* **2003**, *125*, 11822−11823.
(6) Maeda, H.; Furuta, H. *J. Porphyrins Phthalocyanines* **2004**, *8*, 67−75.
(7) Chmielewski, P. J. *Angew. Chem., Int. Ed.* **2004**, *43*, 5655−5658.
(8) Chmielewski, P. J.; Latos-Grazynski, L.; Schmidt, I. *Inorg. Chem.* **2000**, *39*, 5475−5482.
(9) Harvey, J. D.; Ziegler, C. J.; Telser, J.; Ozarowski, A.; Krzystek, J. *Inorg. Chem.* **2005**, *44*, 4451−4453.

10.1021/ic0621852 CCC: $37.00
Published on Web 02/01/2007

Chart 1. Structure of the Two Porphyrin Isomers: (a) [Cu^{II}(TPP)] and (b) [Cu^{II}(NCTPP)]

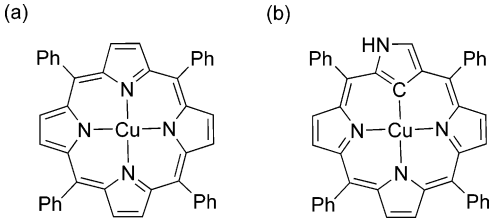

tion spectroscopy (HYSCORE)[10,11] and electron nuclear double resonance (ENDOR),[10,12] we observed an asymmetric spin-density distribution over the three core nitrogen atoms of the NCTPP ligand.[13] However, because of the small natural abundance of ^{13}C (1.1%), the hyperfine coupling of the inner carbon atom could not be observed. Herein we report the results of a CW and pulse EPR study on the copper(II) complex of the ^{13}C-labeled N-confused tetraphenylporphyrin [Cu^{II}(^{13}C-NCTPP)]. The observed ^{13}C hyperfine coupling clearly shows the presence of a σ Cu−C bond and allows for a detailed analysis of the electronic structure of the complex. A comparison between the two structural isomers [Cu^{II}(TPP)] and [Cu^{II}(NCTPP)] shows that in the N-confused complex the covalent character between the metal center and the directly coordinating ligand atoms is much more pronounced. Furthermore, the data analysis is accompanied by supporting density functional theory (DFT) calculations.

Experimental Section

Sample Preparation. The NCP ligand 2-aza-5,10,15,20-tetraphenyl-21-carbaporphyrin ($NCTPPH_2$) was obtained as described by Lindsey and co-workers.[14,15] The ^{13}C-enriched pyrrole needed for the synthesis of the ^{13}C-labeled ligand was obtained following the route described by Williams et al.[16] using [U-^{13}C]galactose as the primary starting material. For details of the synthetic procedures including the metal insertions, see the Supporting Information.

EPR Spectroscopy. CW EPR measurements at X-band were carried out on a Bruker E500 spectrometer equipped with a superhigh Q cavity. Experimental conditions: microwave (mw) frequency, 9.499 GHz; mw power incident to the cavity, 20 mW; modulation frequency, 100 kHz; modulation amplitude, 0.1 mT. Cooling of the sample was performed with a liquid-nitrogen finger Dewar for (T = 150 K).

The liquid-solution CW EPR spectra shown in Figure 4 [diluted in tetrahydrofuran (THF), sample concentration 5 mmol] were recorded with the following experimental conditions: mw frequency, 9.856 GHz; mw power incident to the cavity, 20 mW; modulation frequency, 100 kHz; modulation amplitude, 0.02 mT; sweep width, 80 mT; number of points, 4096.

Pulse EPR measurements at X-band (mw frequency 9.718 GHz) were performed on a Bruker E580 spectrometer at 15 K. The field-swept EPR spectrum (Figure 3, inset) was recorded via the free induction decay (FID) following a pulse length of 500 ns. Davies ENDOR experiments were carried out with the pulse sequence $\pi-T-\pi/2-\tau-\pi-\tau-$echo, with a $\pi/2$ pulse of length 16 ns and a radio-frequency (rf) pulse of length 9 μs during the time T. The triple-resonance spectra of Figure 5 were measured under the same conditions with two rf pulses of length 4.5 μs; the first pulse had a fixed frequency of 30.5 MHz, whereas the frequency of the second pulse was swept between 25 and 85 MHz.

HYSCORE is a pulse EPR method for measuring hyperfine and nuclear quadrupole couplings. This two-dimensional method, with the pulse sequence $\pi/2-\tau-\pi/2-t_1-\pi-t_2-\pi/2-\tau-$echo, correlates nuclear frequencies in one electron spin manifold with nuclear frequencies in the other electron spin manifold. The sensitivity of the HYSCORE experiment can be considerably improved by replacing the second and third $\pi/2$ pulses by matched pulses.[10] The nitrogen-matched HYSCORE spectra of Figure 2 at Q-band (mw frequency 35.3 GHz) were performed on a home-built spectrometer[17] at 20 K and recorded with the following instrumental parameters: $t_{\pi/2} = t_\pi = 16$ ns; strength of matched pulses, $\nu_1 \approx 30$ MHz; length of matched pulses, $t_p = 72$ ns; starting values of the two variable times t_1 and t_2, 24 ns; time increment, $\Delta t = 8$ ns (data matrix 350 × 350); $\tau = 100$ ns. An eight-step phase cycle was used to remove unwanted echoes. The data were processed with the program MATLAB 7.0 (The MathWorks, Natick, MA). The time traces were baseline corrected with a two-order exponential, apodized with a Gaussian window, and zero-filled. After a two-dimensional Fourier transform, the absolute-value spectra were calculated.

The CW EPR and ENDOR spectra were simulated with the *EasySpin* package.[18] HYSCORE spectra were simulated with a program written in-house.[19]

DFT Calculations. Spin-unrestricted geometry optimizations for CuNCTPP (starting structure modified from ref 20) and CuTPP (starting structure taken from ref 21) were done with the Amsterdam Density Functional (ADF 2006.01) package[22] using the BP86 functional with the Becke gradient correction for exchange[23] and the correlation correction by Perdew.[24] During this step, a Slater-type basis set of triple-ζ quality and a single set of polarization functions (TZP, small frozen core) were applied. The single-point calculations omitting the phenyl groups attached to the meso carbons (Cu^{II}NCPor and Cu^{II}Por) for the hyperfine interactions have been carried out using the B3LYP functional and an all-electron triple-ζ basis set with double polarization functions (TZ2P) with the zero-order regular approximation (ZORA).[25] It should be noted that no spin−orbit contribution to the hyperfine interactions was taken into

(10) Schweiger, A.; Jeschke, G. *Principles of Pulse Electron Paramagnetic Resonance*; Oxford University Press: Oxford, U.K., 2001.
(11) Deligiannakis, Y.; Louloudi, M.; Hadjiliadis, N. *Coord. Chem. Rev.* **2000**, *204*, 1−112.
(12) Murphy, D. M.; Farley, R. D. *Chem. Soc. Rev.* **2006**, *35*, 249−268.
(13) Mitrikas, G.; Calle, C.; Schweiger, A. *Angew. Chem., Int. Ed.* **2005**, *44*, 3301−3303.
(14) Geier, G. R.; Haynes, D. M.; Lindsey, J. S. *Org. Lett.* **1999**, *1*, 1455−1458.
(15) Geier, G. R.; Lindsey, J. S. *J. Org. Chem.* **1999**, *64*, 1596−1603.
(16) Williams, S. R.; Maynard, H. D.; Chmelka, B. F. *J. Labelled Compd. Radiopharm.* **1999**, *42*, 927−936.
(17) Gromov, I.; Shane, J.; Forrer, J.; Rakhmatoullin, R.; Rozentzwaig, Y.; Schweiger, A. *J. Magn. Reson.* **2001**, *149*, 196−203.
(18) Stoll, S.; Schweiger, A. *J. Magn. Reson.* **2006**, *178*, 42−55.
(19) Madi, Z. L.; Van Doorslaer, S.; Schweiger, A. *J. Magn. Reson.* **2002**, *154*, 181−191.
(20) Maeda, H.; Osuka, A.; Ishikawa, Y.; Aritome, I.; Hisaeda, Y.; Furuta, H. *Org. Lett.* **2003**, *5*, 1293−1296.
(21) Byrn, M. P.; Curtis, C. J.; Goldberg, I.; Hsiou, Y.; Khan, S. I.; Sawin, P. A.; Tendick, S. K.; Strouse, C. E. *J. Am. Chem. Soc.* **1991**, *113*, 6549−6557.
(22) Velde, G. T.; Bickelhaupt, F. M.; Baerends, E. J.; Guerra, C. F.; Van Gisbergen, S. J. A.; Snijders, J. G.; Ziegler, T. *J. Comput. Chem.* **2001**, *22*, 931−967.
(23) Becke, A. D. *Phys. Rev. A* **1988**, *38*, 3098−3100.
(24) Perdew, J. P. *Phys. Rev. B* **1986**, *33*, 8822−8824.
(25) van Lenthe, E.; Snijders, J. G.; Baerends, E. J. *J. Chem. Phys.* **1996**, *105*, 6505−6516.

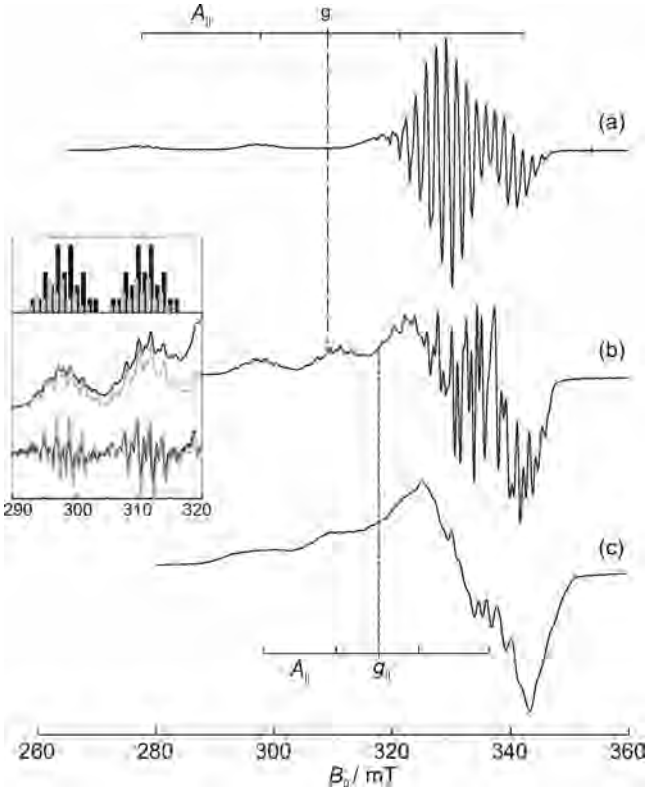

Figure 1. Comparison of the X-band CW EPR spectra of [Cu^{II}TPP] (a), [Cu^{II}NCTPP] (b), and [^{63}Cu^{II}(^{13}C-NCTPP)] (c) diluted in [ZnTPP] powder. The shifts of $g_{||}$ and the corresponding copper hyperfine interactions $A_{||}$ to lower values for [Cu^{II}NCTPP] are clearly visible. The inset shows the magnification of the low-field region of spectrum b and contains the following information: stick spectrum describing the contributions to the observed splitting pattern, ^{63}Cu (black) and ^{65}Cu (gray); the experimental spectrum and its derivative (black) and the corresponding simulations (gray).

account because the current implementation of the B3LYP[26,27] functional in ADF does not allow for this. However, the influence of this neglect has been studied by Saladino and Larsen by applying pure generalized gradient approximation functionals.[28,29]

Results

CW EPR Spectra. The CW EPR spectra of [Cu^{II}NCTPP] and, for comparison reasons, the one of [CuTPP] recorded at X-band mw frequency are shown in Figure 1. Although the [Cu^{II}NCTPP] spectra revealed features that are typical for copper(II) complexes with $d_{x^2-y^2}$ ground state, our previous study showed that the **g** principal values $g_{||} = 2.137 \pm 0.001$ and $g_{\perp} = 2.036 \pm 0.001$ and the ^{63}Cu hyperfine couplings $A_{||} = -(379 \pm 5)$ MHz and $A_{\perp} = +(138 \pm 40)$ MHz are smaller than those of [CuTPP]. The sign of the metal hyperfine couplings given in our present analysis could be determined by the isotropic ^{63}Cu hyperfine coupling obtained from a simulation of the room-temperature spectra of [^{63}Cu^{II}NCTPP] in THF (see Figure 4a, thin line). Additionally, an upper limit of the component $A_{\perp}$ could be derived from spectral simulations of the same compound aligned in a nematic phase (not shown here). Here, features arising only from in-plane interactions could be studied. Nevertheless, a possible rhombic character of the metal hyperfine coupling tensor cannot be excluded.

Our previous study showed that the low-field region of the X-band EPR spectrum exhibits a well-resolved ligand hyperfine structure with the following intensity pattern: 1:1:3:2:5:3:5:2:3:1:1 (Figure 1, inset). Because of an accurate simulation of this part of the spectrum, it was proven that two of the nitrogen donors of the porphyrin core were magnetically equivalent with a hyperfine coupling of $A_{||} \approx 59 \pm 3$ MHz, whereas the third one had a much smaller hyperfine coupling of $A_{||} \approx 29 \pm 3$ MHz.[13]

Upon ^{13}C labeling of the macrocycle, the main features of the EPR spectrum are retained, but there is a considerable line broadening on the order of 5 mT (≈150 MHz) obviously arising from the additional ^{13}C hyperfine splitting (Figure 1c). However, the poor resolution due to the complexity of the CW EPR spectrum does not allow for an accurate determination of the ^{13}C hyperfine couplings.

Interactions of the Three Core ^{14}N Nuclei. A more detailed study of the hyperfine and nuclear quadrupole couplings of the two equivalent nitrogen nuclei in the macrocycle's core is provided by pulse ENDOR spectroscopy. Table 1 summarizes the determined hyperfine couplings from our earlier study.[13]

The hyperfine interactions of the third ^{14}N nucleus of the porphyrin core are observed with HYSCORE spectroscopy at Q-band. This procedure was necessary because in this case the overlapping ^{1}H and ^{14}N ENDOR peaks occurring in X-band experimental spectra could not be well separated using the hyperfine-contrast selectivity method because of baseline imperfections caused by rf heating. In general, ENDOR performed at Q-band would be the method of choice in order to reveal the interactions caused by the third core nitrogen. Unfortunately, technical issues dramatically reduced the sensitivity of the used probehead in this frequency range. Figure 2a shows the single-crystal-like matched HYSCORE spectrum at $g_{||}$. The observed peaks in the shown (−, +) quadrant originate from strong ^{14}N interactions. The cross peaks around (−17, +10) and (−10, +17) MHz are assigned to single-quantum transitions, whereas the two cross peaks at (−33.7, +19.3) and (−19.3, +33.7) MHz are assigned to double-quantum transitions with $\Delta m_I = \pm 2$. The latter transitions are to first-order independent of the nuclear quadrupole interaction, differ by $4\nu_N = 14.4$ MHz, and are centered around the hyperfine coupling of 26.5 MHz along this orientation. The nuclear quadrupole interaction is very small along this orientation, as can be deduced from the modest splitting of the single-quantum peaks. Leaving this orientation and changing the observer position close to $g_{\perp}$ result in a ridgelike-shaped spectrum, shown in Figure 2b. A precise simulation of the spectra at both observer positions allowed for an accurate determination of the spin Hamiltonian parameters: $(A_x, A_y, A_z) = (26.0, 32.6, 26.0)$ MHz for the hyperfine and $(P_x, P_y, P_z) = (+1.10, -0.96, -0.14)$ MHz for the nuclear quadrupole coupling tensors.

(26) Lee, C. T.; Yang, W. T.; Parr, R. G. *Phys. Rev. B* **1988**, *37*, 785−789.
(27) Becke, A. D. *J. Chem. Phys.* **1993**, *98*, 5648−5652.
(28) Saladino, A. C.; Larsen, S. C. *J. Phys. Chem. A* **2003**, *107*, 5583−5587.
(29) Saladino, A. C.; Larsen, S. C. *Catal. Today* **2005**, *105*, 122−133.

Table 1. *g* and *A* Principal Values for [Cu^{II}(NCTPP)] and [Cu^{II}(TPP)][a]

		g_x	g_y	g_z	g_{iso}	ref			
Cu^{II}(NCTPP)		2.036[b]	2.036[b]	2.137[b]	2.070	13			
Cu^{II}(TPP)		2.045	2.045	2.190	2.093	32			
		A_x [MHz]	A_y [MHz]	A_z [MHz]	a_{iso} [MHz]	ρ_s [%]	ρ_p [%]	ref	
Cu^{II}(NCTPP)	^{63}Cu	138 ± 40 (121)	138 ± 40 (163)	−379 ± 5 (−493)	−34 ± 10 (−70)			*d*	
	$^{14}N_{1,3}$	71.5 ± 0.2 (75.3)	58.3 ± 0.2 (61.6)	59.5 ± 0.2 (63.1)	63.1 ± 0.2 (66.7)	4.10 (2.41)	8.33 (6.86)	13	
	$^{14}N_2$	26.0 ± 0.5 (26.8)	32.6 ± 0.5 (33.6)	26.0 ± 0.5 (27.3)	28.2 ± 0.5 (29.2)	1.83 (1.24)	3.67 (3.62)	*d*	
	^{13}C	146 ± 3[c] (158)	189 ± 5[c] (197)	148.5 ± 0.5 (163)	161 ± 1 (173)	5.18 (5.4)	13.92 (14.2)	*d*	
Cu^{II}(TPP)	^{63}Cu	−102.7 (−35.3)	−102.7 (−35.3)	−615 (−730)	−273.5 (−267.0)			32	
	$^{14}N_{1,3}$	54.2 (58.4)	42.8 (46.0)	44.06 (47.2)	47.02 (50.6)	3.05[e] (2.13)	6.37[e] (6.7)	32	
	$^{14}N_{2,4}$	42.8 (46.0)	54.2 (58.4)	44.06 (47.2)	47.02 (50.6)			32	

[a] The **g**-matrix principal values were determined from the simulation of the W-band CW EPR spectrum, while the hyperfine parameters were determined from simulations of ENDOR and HYSCORE spectra. The values in parentheses give the corresponding DFT results for [Cu^{II}(NCPor)] and [Cu^{II}(Por)]. For the definition of the reference system, see Figure 6a. [b] Experimental error ±0.001. [c] Determined from a_{iso} and simulations of ENDOR spectra (Figure 3). [d] This work. [e] Determined with the procedure described here using data of Brown and Hoffman.[32]

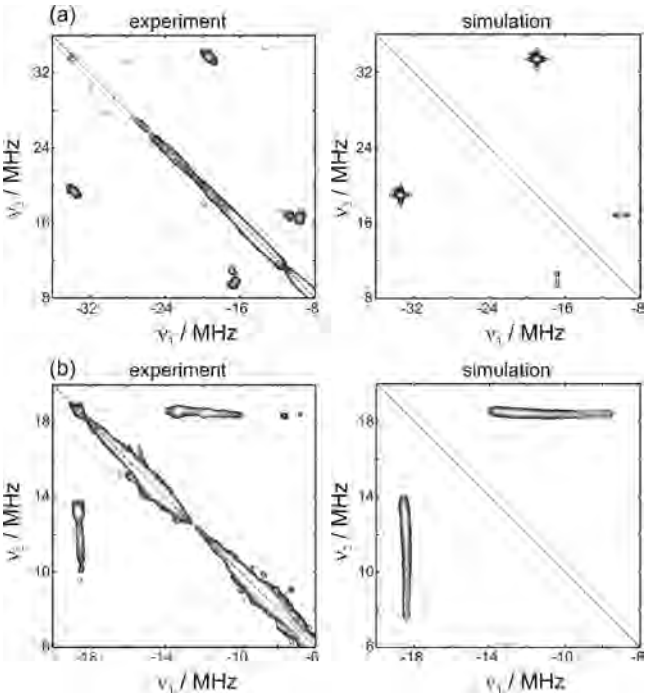

Figure 2. Matched Q-band HYSCORE spectra of [Cu^{II}NCTPP] diluted in [ZnTPP] powder (left) and their simulations (right). (a) Observer position close to $g_{||}$ (both single- and double-quantum correlation peaks are shown). (b) Observer position close to $g_{\perp}$ (only single-quantum correlation ridges are shown). The broad ridges along the diagonal are artifacts originating from the nonideal matched pulses and incomplete transfer of nuclear coherence from the π pulse.

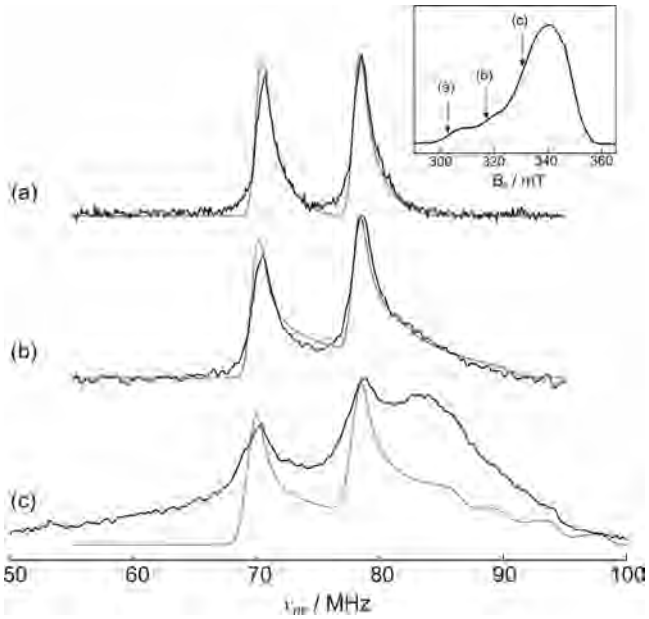

Figure 3. X-band Davies ENDOR spectra of [$^{63}Cu^{II}$(^{13}C-NCTPP)] diluted in [Zn(TPP)] powder measured at different observer positions. Black traces: experiments. Gray traces: simulations (for simulation parameters, see the text). Inset: FID-detected X-band EPR spectrum.

Interactions of the Core ^{13}C Nucleus. Figure 3 shows X-band Davies ENDOR spectra of the ^{13}C-labeled compound measured at different observer positions (Figure 3, inset). The single-crystal-like spectrum measured at $g_{||}$ (trace a) consists of a doublet centered at 75 MHz with the two peaks split by 7.7 MHz, which deviates slightly from twice the ^{13}C Larmor frequency, $2\nu_C = 6.5$ MHz, due to second-order effects. Consequently, these two peaks are assigned to the strongly coupled carbon of the inverted pyrrole. An accurate simulation of this spectrum (Figure 3a, gray trace) gives a hyperfine coupling of 148.5 MHz along this orientation, which is consistent with the line broadening observed in the low-field region of the EPR spectrum (Figure 1c).

Assuming an anisotropic hyperfine interaction, the ENDOR spectra measured at higher magnetic field positions are expected to be broader because of the larger number of orientations contributing to the resonance. This is demonstrated in Figure 3b, where the broadening of the spectrum toward higher frequencies implies an anisotropic hyperfine interaction, with the larger principal value presumably lying in the porphyrin plane, i.e., along the Cu−C bond. However, as the observer position approaches $g_{\perp}$ ($\mathbf{B}_0$ parallel to the porphyrin plane), the ENDOR spectra become very broad because of the contribution of the metal hyperfine interaction ($|A_{||}| = 379$ MHz, $|A_{\perp}| = 138$ MHz). The overlap of the ^{13}C and ^{63}Cu signals (Figure 3c) makes the estimation of the other principal values of the ^{13}C hyperfine coupling tensor virtually impossible.

This difficulty can be overcome if the isotropic hyperfine coupling of ^{13}C can be determined. In principle, this information can be inferred from liquid-solution EPR spectra provided that the rotational correlation time of the molecules is small enough to ensure averaging of the interactions.[30] Figure 4a compares the room-temperature EPR spectra of [$^{63}Cu^{II}$(NCTPP)] and [$^{63}Cu^{II}$(^{13}C-NCTPP)] in THF. For the

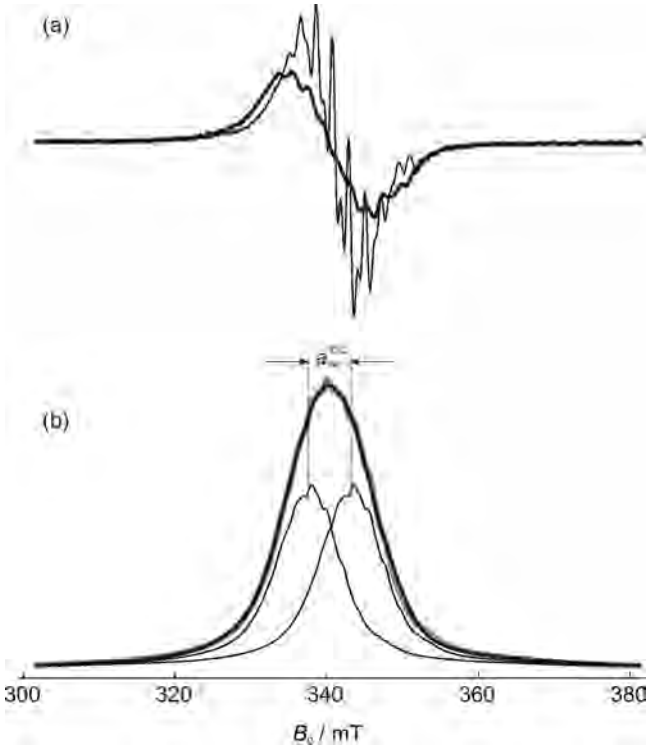

Figure 4. (a) Liquid-solution X-band EPR spectra of [^{63}Cu^{II}(NCTPP)] (thin line) and [^{63}Cu^{II}(^{13}C-NCTPP)] (thick line) diluted in THF ($T = 293$ K). For comparison the spectra are normalized to their double integral. (b) Absorption spectrum of [^{63}Cu^{II}(^{13}C-NCTPP)] (black, thick line) and the corresponding fit (gray, thick line) composed of two absorption [^{63}Cu^{II}-(NCTPP)] spectra of half-intensity, separated by the ^{13}C isotropic hyperfine coupling (thin lines).

non-^{13}C-labeled compound (thin line), the observed signal indicates an unusually small isotropic ^{63}Cu hyperfine interaction. In addition, the superhyperfine ligand splittings are also resolved. More interestingly, upon ^{13}C labeling of the macrocycle (thick line), the spectrum becomes broader, obviously because of the strong ^{13}C hyperfine interaction. It is then straightforward to deduce the isotropic ^{13}C hyperfine coupling, $a_{iso}^{^{13}C}$, by matching the [^{63}Cu^{II}(^{13}C-NCTPP)] spectrum with the sum of two [^{63}Cu^{II}(NCTPP)] spectra of half-intensity, separated by $a_{iso}^{^{13}C}$. During this fitting process, $a_{iso}^{^{13}C}$ was the only varying parameter. A satisfactory agreement occurred when the separation of the two [^{63}Cu^{II}(NCTPP)] spectra was 5.57 ± 0.02 mT, which results in $a_{iso}^{^{13}C} = 161 \pm 1$ MHz (Figure 4b, gray line). By using this information as a constraint and assuming an almost axially symmetric hyperfine interaction, the ^{13}C ENDOR spectra can be best simulated with the principal values $|A_x| = 146 \pm 3$ MHz, $|A_y| = 189 \pm 5$ MHz, and $|A_z| = 148.5 \pm 0.5$ MHz (Figure 3, gray traces).

To decide whether the observed large hyperfine interaction arises from positive (i.e., direct proof of a σ Cu−C bond) or negative (i.e., due to polarization effects) spin population in the ^{13}C orbitals, the sign of the hyperfine coupling has to be known. The relative signs of two hyperfine couplings can be determined by using triple resonance.[31] Figure 5a shows

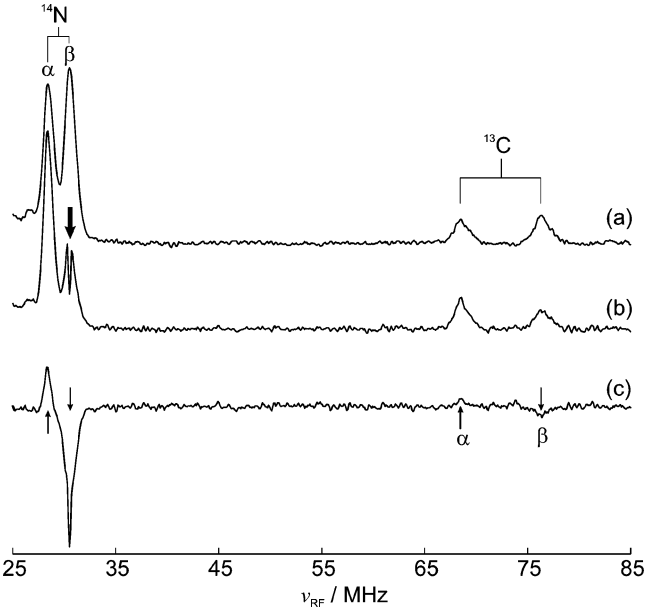

Figure 5. X-band triple resonance of [Cu^{II}(^{13}C-NCTPP)] diluted in [Zn-(TPP)] powder measured at $g_{||}$. (a) Davies ENDOR spectrum. (b) Triple spectrum with $\nu_{rf1} = 30.5$ MHz (marked by the thick arrow). (c) Difference triple spectrum. The arrows indicate positive (up) and negative (down) peaks.

the X-band Davies ENDOR spectrum of the [Cu^{II}(^{13}C-NCTPP)] sample measured at $g_{||}$. Because the ^{14}N hyperfine coupling is positive,[32] the assignment of the nitrogen peaks to the nuclear frequencies of α and β electron spin manifolds is straightforward. The triple-resonance spectrum in Figure 5b is recorded with a fixed rf of $\nu_{rf1} = 30.5$ MHz (marked by the thick arrow), which is resonant with the nitrogen β peak. In the difference triple spectrum (Figure 5c), two negative peaks are observed, namely, the reference peak at 30.5 MHz and the high-frequency ^{13}C peak at 77.6 MHz. Therefore, the latter is assigned to the carbon β peak, and because $g_n^{^{14}N} g_n^{^{13}C} > 0$, we conclude that the ^{13}C hyperfine coupling is positive as well.

The high-resolution data obtained from ENDOR and HYSCORE experiments allow for a detailed analysis of the spin-density distribution over the directly coordinating ligand atoms of the NCTPP macrocycle. Table 1 summarizes the estimated g values and hyperfine couplings together with the corresponding interactions of the [Cu^{II}(TPP)] complex.[32] For comparison, the results of the DFT calculations for [Cu^{II}-(NCPor)] and [Cu^{II}(Por)] are also given in this table (values in parentheses).

Discussion

The interpretation of the magnetic parameters will be made within the molecular orbital (MO) theory framework first used by Maki and McGarvey.[33] The local nuclear configuration consisting of the central Cu^{2+} ion and the directly coordinating ligand atoms having C_{2v} point symmetry is shown in Figure 6a. A possible d orbital splitting is shown in Figure 6b. Assuming a d^9 one-hole system, the electronic

(30) Finazzo, C.; Calle, C.; Stoll, S.; Van Doorslaer, S.; Schweiger, A. *Phys. Chem. Chem. Phys.* **2006**, *8*, 1942−1953.
(31) Mehring, M.; Höfer, P.; Grupp, A. *Ber. Bunsenges. Phys. Chem.* **1987**, *91*, 1132−1137.
(32) Brown, T. G.; Hoffman, B. M. *Mol. Phys.* **1980**, *39*, 1073−1109.
(33) Maki, A. H.; McGarvey, B. R. *J. Chem. Phys.* **1958**, *29*, 31−34.

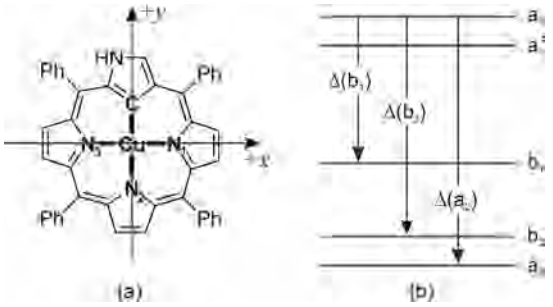

Figure 6. (a) Reference system with the Cu^{2+} ion placed at the origin. The *y* axis is the C_2 axis of the local C_{2v} symmetry. (b) Possible d orbital splitting.

states will be described by the set of basis functions describing antibonding MOs

$$|a_1\rangle = \alpha\Phi_{a1} - \alpha'_{N1}\sigma_{N13} - \alpha'_{N2}\sigma_{N2} - \alpha'_C\sigma_C$$

$$|b_1\rangle = \beta\Phi_{b1} - \beta'_{N1}\pi^y_{N13} - \beta'_{N2}\pi^x_{N2} - \beta'_C\pi^x_C$$

$$|b_2\rangle = \gamma_2\Phi_{b2} - \gamma'_{2N2}\pi^z_{N2} - \gamma'_{2C}\pi^z_C$$

$$|a_2\rangle = \gamma_1\Phi_{a2} - \gamma'_{1N13}\pi^z_{N13}$$

$$|a'_1\rangle = \delta\Phi_{a1'} - \delta'_{N1}\sigma'_{N13} - \delta'_{N2}\sigma'_{N2} - \delta'_C\sigma'_C \qquad (1)$$

where

$$\Phi_{a_1} = c_1 d_{x^2-y^2} + c_2 d_{z^2} + c_s s$$

$$\Phi_{b_1} = d_{xy}$$

$$\Phi_{b_2} = d_{yz}$$

$$\Phi_{a_2} = d_{xz}$$

$$\Phi_{a_1'} = c_1 d_{z^2} - c_2 d_{x^2-y^2} + c'_s s \qquad (2)$$

denote one-electron atomic orbitals (AOs) centered at the central copper nucleus and

$$\begin{array}{lll}
\sigma_{N13} = (1/\sqrt{2})[-\sigma_x(1) + \sigma_{x'}(3)] & \sigma_{N2} = -\sigma_y(2) & \sigma_C = \sigma_y(4) \\
\pi^y_{N13} = (1/\sqrt{2})[\pi_y(1) - \pi_y(3)] & \pi^x_{N2} = -\pi_x(2) & \pi^x_C = \pi_x(4) \\
\pi^z_{N13} = (1/\sqrt{2})[\pi_z(1) - \pi_z(3)] & \pi^z_{N2} = -\pi_z(2) & \pi^z_C = \pi_z(4) \\
\sigma'_{N13} = (1/\sqrt{2})[\sigma_x(1) - \sigma_{x'}(3)] & \sigma'_{N2} = -\sigma_y(2) & \sigma'_C = \sigma_y(4)
\end{array} \qquad (3)$$

denote normalized linear combinations of AOs centered at the ligand with the following definitions:

$$\sigma_i = n(2p_i) + \sqrt{1-n^2}(2s) \quad \text{and}$$

$$\sigma_{i'} = n(2p_i) - \sqrt{1-n^2}(2s) \quad \text{with } i = x, y$$

$$\pi_i = (2p_i) \quad \text{with } i = x, y, z \qquad (4)$$

In eq 4, *n* denotes the hybridization parameter (for a schematic representation of the AOs, see Figure S1 in the Supporting Information).

Metal-Dominated EPR Parameters. The *g* values (for simplification reasons, ignoring ligand AOs) are given by[34]

$$g_x = g_e + \Delta g_x = 2.0023 + [2\alpha^2\gamma_2^2(c_1 + \sqrt{3}c_2)^2]\xi/\Delta(b_2)$$

$$g_y = g_e + \Delta g_y = 2.0023 + [2\alpha^2\gamma_1^2(c_1 - \sqrt{3}c_2)^2]\xi/\Delta(a_2)$$

$$g_z = g_e + \Delta g_z = 2.0023 + 8\alpha^2\beta^2 c_1^2\xi/\Delta(b_1) \qquad (5)$$

where $\xi = 830\ cm^{-1}$ is the Cu^{2+} spin−orbit coupling and $\Delta(a_2)$, $\Delta(b_1)$, and $\Delta(b_2)$ denote positive energy differences, as shown in Figure 6b. The ^{63}Cu hyperfine couplings are given by[34]

$$A_x = A_{4s}\alpha^2 c_s^2 + P\left[-\alpha^2\kappa + \frac{2}{7}\alpha^2(c_1^2 - c_2^2 - 2\sqrt{3}c_1c_2) + \Delta g_x - \frac{1}{14}\frac{3c_1 + \sqrt{3}c_2}{c_1 - \sqrt{3}c_2}\Delta g_y + \frac{\sqrt{3}}{14}\frac{c_2}{c_1}\Delta g_z\right]$$

$$A_y = A_{4s}\alpha^2 c_s^2 + P\left[-\alpha^2\kappa + \frac{2}{7}\alpha^2(c_1^2 - c_2^2 + 2\sqrt{3}c_1c_2) - \frac{1}{14}\frac{3c_1 - \sqrt{3}c_2}{c_1 + \sqrt{3}c_2}\Delta g_x + \Delta g_y - \frac{\sqrt{3}}{14}\frac{c_2}{c_1}\Delta g_z\right]$$

$$A_z = A_{4s}\alpha^2 c_s^2 + P\left[-\alpha^2\kappa - \frac{4}{7}\alpha^2(c_1^2 - c_2^2) + \frac{1}{14}\frac{3c_1 - \sqrt{3}c_2}{c_1 + \sqrt{3}c_2}\Delta g_x + \frac{1}{14}\frac{3c_1 + \sqrt{3}c_2}{c_1 - \sqrt{3}c_2}\Delta g_y + \Delta g_z\right] \qquad (6)$$

where $-P\alpha^2\kappa$ and $A_{4s}\alpha^2 c_s^2$ are the isotropic hyperfine couplings due to spin polarization and contribution of the 4s metal orbital, respectively. As can be easily seen, eq 6 reduces to the expression for the D_{4h} case when $c_2 = 0$ apart from the $A_{4s}\alpha^2 c_s^2$ term. In eq 6, $P = (\mu_0/4\pi h)g_e g_n^{^{63}Cu}\beta_e\beta_n\langle r^{-3}\rangle_{3d} = 1171$ MHz is the dipolar hyperfine coupling and $A_{4s} = (8\pi/3)(\mu_0/4\pi h)g_e g_n^{^{63}Cu}\beta_e\beta_n|\Psi_{4s}(0)|^2 = 3559$ MHz is the isotropic hyperfine coupling for an electron in the copper 4s orbital.[35] The ^{63}Cu isotropic hyperfine coupling is given by

$$A_{iso}^{Cu} = A_{4s}\alpha^2 c_s^2 + P\left[-\alpha^2\kappa + \frac{1}{3}(\Delta g_x + \Delta g_y + \Delta g_z)\right] \qquad (7)$$

Because of the C_{2v} symmetry, mixing of the $3d_{x^2-y^2}$, $3d_{z^2}$, and 4s metal orbitals is allowed (eq 2). The contribution of 4s accounts for the increased isotropic metal hyperfine coupling observed experimentally. A possible contribution

(34) Mabbs, F.; Collison, D. *Studies in Inorganic Chemistry 16: Electron Paramagnetic Resonance of d Transition Metal Compounds*; Elsevier: London, 1992.
(35) Koh, A. K.; Miller, D. J. *At. Data Nucl. Data Tables* **1985**, *33*, 235−253.

of $3d_{z^2}$ ($c_2 \neq 0$) would lead to a rhombic g and metal hyperfine coupling tensors (eqs 5 and 6). Although an axial g tensor was observed, eq 5 depends on too many unknown parameters and therefore does not allow for a definite estimation of c_2. However, from eq 6, we find

$$A_x - A_y = P\left(-\frac{8\sqrt{3}}{7}\alpha^2 c_1 c_2 + \frac{2\sqrt{3}}{14}\frac{c_2}{c_1}\Delta g_z - \frac{8\sqrt{3}}{14}\frac{c_1 c_2}{{c_1}^2 - 3{c_2}^2}\Delta g_x\right) \quad (8)$$

Equation 8 can be used in order to estimate the upper limit of a possible $3d_{z^2}$ contribution because the maximum difference $|A_x - A_y|$ is experimentally found to be smaller than 45 MHz. Assuming $\alpha^2 = 0.6$, which is an usual covalency parameter found for copper in the porphyrin-like environment,[32] it is concluded (see Figure S2 in the Supporting Information) that ${c_2}^2$ cannot be larger than 0.1% in order to account for a possible rhombic deviation of the metal hyperfine coupling, which cannot be excluded within the experimental error. Therefore, in the following analysis, c_2 was set to 0.

Equation 7 can be used in order to estimate the contribution of the copper 4s orbital, c_s. However, the empirical parameter κ describing the contribution of the core polarization to the isotropic hyperfine coupling is involved in eq 7. Because the contribution of the core polarization is not supposed to dramatically change upon changing the ligand system from TPP to NCTPP, we have used the value $\kappa = 0.4559$, deduced from ref 32.

Ligand Hyperfine Couplings. For a σ orbital involving an arbitrary ligand atom N in the first coordination sphere and pointing along the metal−ligand direction (principal axis g_x, for example, atoms N_1 and N_3 in Figure 6a), the principal values of the ligand hyperfine tensor are given by[36]

$$A_x^N = a_{iso}^N(2s) + A_{||}^N(2p_x) + A_x^N(D) + A_\perp^N(2p_z)$$

$$A_y^N = a_{iso}^N(2s) + A_\perp^N(2p_x) + A_y^N(D) + A_\perp^N(2p_z)$$

$$A_z^N = a_{iso}^N(2s) + A_\perp^N(2p_x) + A_z^N(D) + A_{||}^N(2p_z) \quad (9)$$

In the above expressions, the first terms are the isotropic hyperfine coupling (s character of the σ bond), the second terms give the through-bond anisotropic hyperfine coupling (p character of the σ bond), and the third terms describe the through-space dipolar interaction. The last terms are introduced to take into account a possible orthorhombic hyperfine tensor found experimentally, indicating a contribution of out-of-plane π bonding. The terms are defined by

$$a_{iso}^N(2s) = \frac{8\pi}{3}P_N|\Psi_{2s}^N(r_N{=}0)|^2(1 - {n_N}^2){\alpha'_N}^2 \quad (10)$$

$$\begin{pmatrix} A_{||}^N(2p_x) \\ A_\perp^N(2p_x) \\ A_\perp^N(2p_x) \end{pmatrix} = P_N\langle {r_N}^{-3}\rangle_{2p} {n_N}^2 {\alpha'_N}^2 \begin{pmatrix} {}^4/_5 \\ -{}^2/_5 \\ -{}^2/_5 \end{pmatrix} \quad (11)$$

$$\begin{pmatrix} A_x^N(D) \\ A_y^N(D) \\ A_z^N(D) \end{pmatrix} = P_N\frac{1}{{R_N}^3}\begin{pmatrix} 2(\alpha^2 + \Delta g_x/g_e) \\ -(\alpha^2 + \Delta g_y/g_e) \\ -(\alpha^2 + \Delta g_z/g_e) \end{pmatrix} \quad (12)$$

where P_N is given by $P_N = (\mu_0/4\pi h)g_e g_N \beta_e \beta_n$, n_N is the hybridization parameter (eq 4), α'_N is the covalency parameter of atom N (eq 1), and R_N is the Cu^{2+}−N distance. The quantities $\rho_{2s}^N(0) \equiv |\Psi_{2s}^N(r_N{=}0)|^2$ and $\langle {r_N}^{-3}\rangle_{2p}$ depend on the choice of the AO. Table S1 (see the Supporting Information) gives the numerical values we used in the present work, calculated with the AOs given by Clementi.[37] These values are the same as the ones given by Koh and Miller.[35]

Estimation of Bonding Parameters. Combined with the experimental data, eqs 9−12 can be used for the estimation of the bonding parameters n and α' and the spin populations $\rho_s = (1 - n^2)\alpha'^2$ and $\rho_p = n^2\alpha'^2$ of the ligand atoms in the first coordination sphere. However, because the *unknown* covalency parameter α (contribution of the metal AO) is involved in the through-space dipolar part of the hyperfine coupling (see eq 12), an accurate solution of the problem requires the implementation of an iterative procedure. During this, the bonding parameters should form a self-consistent solution for eqs 9−12. In addition, the following normalization condition should be fulfilled:

$$\alpha^2 + {\alpha'_{N1}}^2 + {\alpha'_{N2}}^2 + {\alpha'_C}^2 - \alpha\alpha'_{N1}\langle\Phi_{a1}|\sigma_{N13}\rangle - \alpha\alpha'_{N2}\langle\Phi_{a1}|\sigma_{N2}\rangle - \alpha\alpha'_C\langle\Phi_{a1}|\sigma_C\rangle = 1 \quad (13)$$

where overlap integrals between ligand AO have been omitted. To use eq 13, the three overlap integrals $\langle\Phi_{a1}|\sigma_{N13}\rangle$, $\langle\Phi_{a1}|\sigma_{N2}\rangle$, and $\langle\Phi_{a1}|\sigma_C\rangle$ have to be calculated (see the Supporting Information). In this work, three different cases of ligand valence states have been considered: (1) all atoms were considered to be neutral; (2 and 3) a doubly positively charged copper atom with two negatively charged ligand atoms (either $N_{1,3}$ or N_2 and C) has been assumed. These limiting cases sufficiently describe the "real" situation. The necessary overlap integrals between metal and ligand AOs used in the present analysis are given in Table S2 of the Supporting Information. The AOs have been constructed using the expansion coefficients and orbital exponents given in ref 37. The distances $R_{N1,N3} = 2.07$ Å, $R_{N2} = 2.02$ Å, and $R_C = 1.96$ Å used for the calculation of the overlap integrals were taken from a DFT-based geometry optimization.

Following a similar procedure applied by Lorenz and Günthard,[38] the bonding parameters were estimated using eqs 9−12, the normalization condition (eq 13), the constraint ${c_1}^2 + {c_s}^2 = 1$, and eq 7 describing the isotropic hyperfine

(36) Schweiger, A. *Struct. Bonding* 1982, *51*, 1−119.

(37) Clementi, E. *IBM J. Res. Dev.* **1965**, *9*, 2, supplement.

(38) Lorenz, A. R.; Günthard, H. H. *Chem. Phys.* **1976**, *14*, 327−344.

Table 2. Bonding Parameters (Hybridization Coefficients) for the [Cu^{II}(NCTPP)] Complex

	Cu ($N_{1,3}$, N_2, C)	Cu^{2+} ($N_{1,3}$, N_2^{-1}, C^{-1})	Cu^{2+} ($N_{1,3}^{-1}$, N_2, C)
α^2	0.6191	0.5293	0.4974
c_1^2	0.9012	0.9099	0.9138
c_s^2	0.0988	0.0901	0.0862
α'^2_{N1}	0.2486	0.2510	0.3096
n_{N1}	0.8188	0.8208	0.8478
α'^2_{N2}	0.0550	0.0692	0.0567
n_{N2}	0.8167	0.8478	0.8230
α'^2_C	0.1909	0.2512	0.1945
n_C	0.8537	0.8792	0.8566
$\langle\Phi_{a1}\|\sigma_{N13}\rangle$	−0.0072	−0.0396	−0.0785
$\langle\Phi_{a1}\|\sigma_{N2}\rangle$	0.1994	0.1881	0.1646
$\langle\Phi_{a1}\|\sigma_C\rangle$	0.2316	0.2170	0.1973

Table 3. Calculated Spin Populations (%) at Ligand Atoms[a] and sp^n Hybridizations (ρ_p/ρ_s) Using the Values of Table 2

	Cu ($N_{1,3}$, N_2, C)	Cu^{2+} ($N_{1,3}$, N_2^{-1}, C^{-1})	Cu^{2+} ($N_{1,3}^{-1}$, N_2, C)
$\rho_s^{N_{1,3}}$	4.10	4.10	4.35
$\rho_p^{N_{1,3}}$	8.33	8.46	11.13
$\rho_p^{N_{1,3}}/\rho_s^{N_{1,3}}$	2.03	2.06	2.56
$\rho_s^{N_2}$	1.83	1.94	1.83
$\rho_p^{N_2}$	3.67	4.97	3.84
$\rho_p^{N_2}/\rho_s^{N_2}$	2.00	2.56	2.10
ρ_s^C	5.18	5.70	5.18
ρ_p^C	13.92	19.41	14.27
ρ_p^C/ρ_s^C	2.69	3.40	2.76
$\rho^{L\,b}$	49.45	57.14	56.08

[a] Spin populations were calculated as follows: for atoms N_1 and N_3, $\rho_s^{N_{1,3}} = (1/2)(1 - n_{N1}^2)\alpha'^2_{N1}$ and $\rho_p^{N_{1,3}} = 1/2\, n_{N1}^2\alpha'^2_{N1}$; for atoms N_2 and C, $\rho_s^{N_2,C} = (1 - n_{N2,C}^2)\alpha'^2_{N2,C}$ and $\rho_p^{N_2,C} = n_{N2,C}^2\alpha'^2_{N2,C}$. [b] Total spin population at the four directly coordinated ligand atoms.

coupling of the metal. The results are summarized in Table 2. In addition, the spin populations and hybridizations of the ligand atoms are listed in Table 3.

From Table 2, an upper limit of the contribution of the copper $3d_{x^2-y^2}$ orbital to the singly occupied MO (SOMO) can be estimated to be $\alpha^2 c_1^2 = 0.558$, representing the maximum possible spin population in this orbital, neglecting the overlap with the ligand. In a similar fashion, the maximum contribution arising from the 4s orbital is found to be $\alpha^2 c_s^2 = 0.06$. It can be seen that the ligand bond hybridization deviates more from the sp^2 value if the charge of the involved atom is taken as negative. In this respect, the best agreement is reached for the case where all atoms have been considered uncharged. The performed DFT computation resulted in the following charge distribution based on a Mulliken population analysis: +0.5 on the central copper atom, each −0.5 on the three core nitrogen atoms, and −0.2 on the inverted carbon atom. This leads to a situation best described by a superposition of the two latter cases. The hereafter obtained bond hybridizations well agree with the DFT findings, resulting in hybridizations of approximately 2.3−2.4 for the metal−nitrogen bonds and 3 for the carbon. Taking into account core polarization for the ligand atoms and including π bonding reduce these experimental hybridization ratios noticeably[32] but do not affect the relative differences between the nitrogen nuclei and the carbon nucleus. Therefore, because actually the 4s contribution is not described in the Slater-type orbitals used in the Cu^{2+} case (we had to use the 4s functions of the neutral copper), we chose case 1 to be the most appropriate in the following discussion.

Table 4. Bonding Parameters (Hybridization Coefficients) for the [Cu^{II}(TPP)] Complex, Calculated Spin Populations (%) at Ligand Atoms, and sp^n Hybridization (ρ_p/ρ_s) Using the Data of Brown and Hoffman[32]

α^2	0.7033	ρ_s^N	3.05
α'^2_N	0.1885	ρ_p^N	6.37
n_N	0.8223	ρ_p^N/ρ_s^N	2.09
		ρ^L	37.71

On the basis of the above results, the hyperfine principal values of the directly coordinating ligand atoms can be written as

$$^{14}N_{1,3}: \begin{bmatrix}71.5\\58.3\\59.5\end{bmatrix} = 63.1 + \begin{bmatrix}7.97\\-3.98\\-3.98\end{bmatrix} + \begin{bmatrix}0.82\\-0.41\\-0.44\end{bmatrix} + \begin{bmatrix}-0.40\\-0.40\\0.80\end{bmatrix} \text{MHz} \quad (14a)$$

$$^{14}N_2: \begin{bmatrix}26.0\\32.6\\26.0\end{bmatrix} = 28.2 + \begin{bmatrix}-1.75\\3.51\\-1.75\end{bmatrix} + \begin{bmatrix}-0.44\\0.88\\-0.48\end{bmatrix} + \begin{bmatrix}0\\0\\0\end{bmatrix} \text{MHz} \quad (14b)$$

$$^{13}C: \begin{bmatrix}146.0\\189.0\\148.5\end{bmatrix} = 161.2 + \begin{bmatrix}-12.63\\25.26\\-12.63\end{bmatrix} + \begin{bmatrix}-1.68\\3.36\\-1.81\end{bmatrix} + \begin{bmatrix}-0.83\\-0.83\\1.67\end{bmatrix} \text{MHz} \quad (14c)$$

where the order of the terms follows the definition of eq 9. From eq 14, it is concluded that the main contribution to the through-bond anisotropic hyperfine coupling arises from p-character σ bonding (second terms). No contribution from in-plane π bonding is found, whereas the last terms show a significant contribution from out-of-plane π bonding for the two magnetically equivalent nitrogens ($N_{1,3}$) and the carbon nucleus.

To compare these results with the [Cu^{II}(TPP)] case, we analyzed the data of Brown and Hoffman[32] in the same fashion. The data are shown in Table 4. The comparison shows that in the case of [Cu^{II}(NCTPP)] there is at least 11% more spin population on the porphyrin macrocycle. This result indicates that in the NCP complex the metal−ligand bond has in total stronger covalent character, in agreement with the experimentally observed smaller g_z. In addition, the analysis of the bonding parameters shows that the covalency factors of the ligand atoms, α', follow the order $\alpha_{N2}' < \alpha_{N1}' < \alpha_C'$. This clearly shows that in the [Cu^{II}(NCTPP)] complex the Cu−C bond is the strongest among the other metal−ligand bonds. Furthermore, using eq 5 for g_z and the covalency parameters α^2, c_1^2, and $\beta^2 \approx 1$ (because no in-plane π bonding was found), an energy difference $\Delta(b_1)$ of

27 503 cm^{-1} can be inferred. This value is considerably larger than the one found for [Cu^{II}(TPP)],[32] indicating a stronger perturbation of the $3d_{x^2-y^2}$ orbital. This finding is in agreement with the larger covalent character already mentioned.

Upon comparison of the computational results obtained for [CuPor] and [CuNCPor], the same trend concerning the covalent character as that for the experiment is observed: Changing the ligand system to the N-confused macrocycle reduces the spin population on the central metal ion from 61% to 55.4% and introduces an asymmetry of the spin populations of the ligand. Furthermore, a 2% contribution of metal 4s character in the SOMO has been predicted as well. However, it should be noted that the experimentally observed increase of the unpaired electron population of 11% on the directly coordinating ligand nuclei cannot be accurately reproduced (DFT finds 7.7%). The sign prediction of the hyperfine couplings arising from directly coordinating atoms, as well as their orientation, is in accordance with our experiments and earlier results.[32] The main deviation between the experimentally determined and computed hyperfine parameters can be identified to be the isotropic hyperfine coupling (Table 1). This overestimation is inherent to DFT methods generally tending to overestimate the covalency[39] even upon inclusion of Hartree−Fock exchange. Furthermore, the experimental finding that in the CuNCTPP complex the Cu−C bond is the strongest among the other metal−ligand bonds is supported by a Mayer bond-order analysis based on the DFT results: Here we find a bond order of 0.88 describing the metal−carbon bond, whereas the metal−nitrogen bond orders are found to be between 0.41 and 0.44.

(39) Neese, F. *Magn. Reson. Chem.* **2004**, *42*, S187−S198.

Conclusion

In summary, we have presented a detailed CW and pulse EPR study of the [Cu^{II}(NCTPP)] complex. The observed hyperfine couplings of the ligand atoms in the first coordination sphere showed the presence of a remarkably strong σ Cu−C bond and allowed for a detailed analysis of the spin delocalization over the porphyrin macrocycle. Interestingly, the observed delocalization is approximately 11% larger than the corresponding one of [Cu^{II}(TPP)]. Furthermore, the above analysis revealed a noticeable contribution ($\approx$6%) of the metal 4s orbital to the SOMO, which is allowed in C_{2v} symmetry and accounts for the observed larger ^{63}Cu isotropic hyperfine coupling. A possible contribution of the metal $3d_{z^2}$ orbital (also allowed in C_{2v} symmetry) cannot be excluded; however, on the basis of the experimental data, it is expected to be very modest because our analysis gave an upper limit of approximately 0.06%.

To the best of our knowledge, copper complexes with NCP ligand derivatives belong to the very rare examples of stable monomeric organometallic copper(II) species. Our results show how powerful pulse EPR methods can be in characterizing the bonding situation of paramagnetic transition-metal-containing complexes.

Acknowledgment. This work was supported by the Swiss National Science Foundation. We thank Bruno Mancosu for preparing the NCTPP ligand.

Supporting Information Available: Figures S1 and S2, Tables S1 and S2, and sample preparation details. This material is available free of charge via the Internet at htpp://pubs.acs.org.

IC0621852